Three-dimensional momentum-resolved electronic structure of 1*T*-$TiSe_2$: A combined soft-x-ray photoemission and density functional theory study

Z. Vydrova,[1] E. F. Schwier,[2] G. Monney,[1] T. Jaouen,[1] E. Razzoli,[1] C. Monney,[3] B. Hildebrand,[1] C. Didiot,[1] H. Berger,[4] T. Schmitt,[5] V. N. Strocov,[5] F. Vanini,[1] and P. Aebi[1]

[1]*Département de Physique and Fribourg Center for Nanomaterials, Université de Fribourg, CH-1700 Fribourg, Switzerland*
[2]*Hiroshima Synchrotron Radiation Center, Hiroshima University, 2-313 Kagamiyama, Higashi-Hiroshima 739-0046, Japan*
[3]*Department of Physics, University of Zurich, Winterthurerstrasse 190, 8057 Zurich, Switzerland*
[4]*Institut de Physique de la Matière Complexe, EPFL, CH-1015 Lausanne, Switzerland*
[5]*SLS, Paul Scherrer Institute, CH-5232, Villigen PSI, Switzerland*

(Received 31 March 2015; revised manuscript received 3 June 2015; published 16 June 2015)

1*T*-$TiSe_2$ is a quasi-two-dimensional transition metal dichalcogenide, which exhibits a charge density wave transition at a critical temperature of ∼200 K as well as low-temperature superconductivity induced by pressure or intercalation. The electronic energy dispersion measured by soft x-ray angle-resolved photoemission is not only momentum resolved parallel to the surface but also perpendicular to it. Experiments are compared to density functional theory based band structure calculations using different exchange-correlation functionals. The results reveal the importance of including spin-orbit coupling for a good description of the experimental bands. Compared to calculations within the local density approximation, the use of the modified Becke-Johnson (mBJ) exchange functional leads to a band structure that does not need an artificial downwards shift of the valence band to fit the experiment. The mBJ functional thus clearly appears as the most adapted functional for the theoretical description of the 1*T*-$TiSe_2$ band structure within the DFT framework.

DOI: 10.1103/PhysRevB.91.235129 PACS number(s): 71.20.−b, 79.60.−i, 71.15.Mb

I. INTRODUCTION

Transition metal chalcogenides (TMDC) recently attracted strong interest in the context of various topics including quantum phase and metal-insulator transitions as well as superconductivity [1,2]. In particular, 1*T*-$TiSe_2$ is a quasi-two-dimensional (2D) transition metal dichalcogenide which exhibits a phase transition towards a commensurate ($2 \times 2 \times 2$) charge density wave (CDW) [3,4] and an expected excitonic insulator [5–7] phase below ∼200 K. In the past few years, it has attracted a renewed interest due to the discovery of a superconducting phase induced by pressure [8], or by Cu atom intercalation [9], and a proposed chiral-type of the CDW [10–12].

Although 1*T*-$TiSe_2$ is a quasi-2D-material, parts of its electronic structure exhibit three-dimensional (3D) character and its precise band structure is not truly known. Many angle-resolved ultraviolet (UV) photoemission experiments have been carried out (for a review see, e.g., Refs. [13,14]), but complementary soft x-ray angle-resolved photoemission spectroscopy (SX-ARPES) experiments are lacking so far. At soft x-ray photon energies, the photoelectron mean free path is larger, thereby minimizing the intrinsic limit of the UV ARPES measurement's surface sensitivity and momentum-resolution perpendicular to the surface (k_z) [15–17]. Therefore SX-ARPES experiments give access to the bulk electronic structure of the material with high resolution in k_z and allow to compare the experimental data to extended band-structure calculations.

With respect to experiments reporting a chiral CDW phase in 1*T*-$TiSe_2$ and the presence of electron correlation effects via the formation of electron-hole pairs (excitons), it is of great interest to investigate the strength of spin-orbit (SO) and band renormalization effects, respectively. In the case of SO coupling, it is well known that degenerate energy levels may split, and if inversion symmetry is broken, spin-split bands may appear [18]. Previously, SO effects have been identified in the transition metal dichalcogenides 1*T*-TaS_2 and 1*T*-$TaSe_2$ [19]. DFT calculations have been applied to the CDW phase of 1*T*-$TiSe_2$ by Zhu *et al.* [20] in order to investigate the origin of the CDW, and have shown a strong dependence of the total energy on the exchange-correlation functional indicating a crucial role of electron correlations.

In this paper, we present SX-ARPES measurements of the 1*T*-$TiSe_2$ band structure performed for different photon energies, probing different high symmetry planes in the Brillouin zone (BZ). We compare our experimental results to extensive band structure calculations within the DFT framework and using different exchange-correlation functionals. Our results demonstrate the importance of SO coupling in 1*T*-$TiSe_2$ and reveal that the choice of the exchange-correlation functional is determinant for a good description of its electronic band structure by DFT.

II. EXPERIMENT AND CALCULATIONS

The electronic structure of 1*T*-$TiSe_2$ has been measured at the soft x-ray ARPES endstation of the advanced resonant spectroscopies (ADRESS) beamline at the Swiss Light Source. The description of the experimental geometry can be found elsewhere [15,17]. The slit of the analyser PHOIBOS-150 was oriented perpendicular to the incident x rays. The total experimental resolution was ∼120 meV. The sample was cleaved *in situ* at 11 K. The experiments probed the electronic structure in the LAΓM plane of the BZ (see inset of Fig. 1) using photon energies in steps of 10 eV in the range from 910 to 990 eV. Evaluating the symmetry and shifts in the band positions of the measured data, the *M*-Γ and *L*-*A* paths are probed by using 910 and 980 eV photon energy, respectively. Although

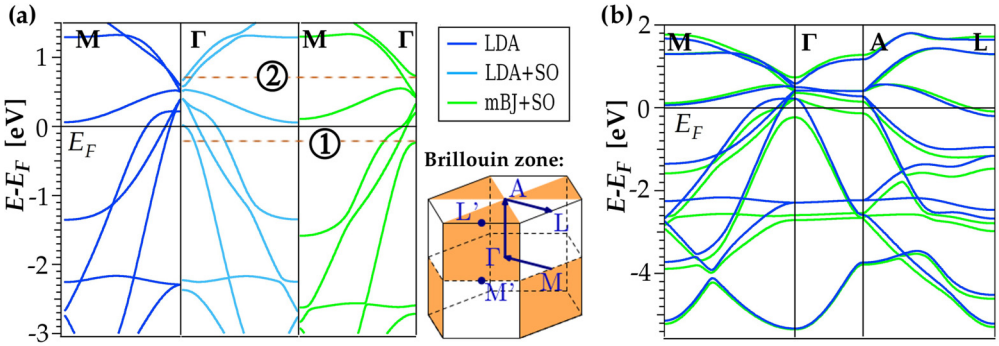

FIG. 1. (Color online) Band-structure calculations of the $(1 \times 1 \times 1)$ unreconstructed bulk unit cell of $1T$-$TiSe_2$. (a) Comparison of the band structure along the ΓM path obtained with the different exchange-correlation functionals. Dashed brown lines mark the effect of the mBJ exchange functional on the band gap, increasing the separation of occupied and unoccupied bands. (b) Full band structure calculated using LDA and mBJ exchange-correlation functionals, the latter with SO coupling.

the measurements have been done at low temperature, in the CDW phase, the bands follow well the calculations of the original unreconstructed structure (see below).

The DFT calculations have been performed using the WIEN2K package [21] by considering different exchange-correlation functionals implemented within this package, namely the local density approximation (LDA) [22], the generalized gradient approximation (GGA), and a combination of the modified Becke-Johnson exchange potential (mBJ) and the LDA approximation of the correlation potential [23]. In fact, the mBJ functional is an approach that has demonstrated the ability to predict band gaps and band orders with the same accuracy as computationally expensive GW calculations [23]. This has been confirmed for the two transition metal dichalcogenides TiS_2 and $TiTe_2$ [24].

All functionals have been used with and without SO coupling and the calculations carried out for the nonreconstructed structure (normal phase) using the tabulated experimental values of the $1T$-$TiSe_2$ structure [25]. The lattice parameters of the primitive cell were set to $a = b = 3.54$ Å and $c = 6.008$ Å and the position of the atoms within the structure were (0,0,0) and (1/3,2/3,0.25504) for Ti and Se, respectively. $1T$-$TiSe_2$ crystallizes in the $P\bar{3}m1$ space group (No. 164), with a hexagonal BZ exhibiting threefold symmetry with respect to c axis [see inset of Fig. 1(a), where symmetry equivalent regions of the BZ are marked]. Additional parameters used for calculation are the threshold energy of 6.0 Ry separating the valence from the core states, the muffin-tin radius $R_{MT(Ti)} = 2.5$ bohr for Ti and $R_{MT(Se)} = 2.26$ bohr for Se. A mesh of 10 000 k points was used in all cases.

III. RESULTS AND DISCUSSION

Figure 1 presents the DFT-calculated band structure obtained by using the LDA, the LDA + SO, and the mBJ + SO exchange-correlation functionals. Figure 1(a) shows a detailed comparison of the effects of the different functional on the electronic bands for the ΓM path, whereas part (b) displays the overall band structure calculation for the two most different cases (i.e., LDA and mBJ + SO).

According to the DFT-LDA electronic structure, $TiSe_2$ is metallic with a band overlap of 0.6 eV between the top of the hole pocket at Γ and the bottom of the electron pocket at L [see Fig. 1(b)]. Including SO coupling [center panel of Fig. 1(a)], does not change the valence-conduction bands overlap, but at Γ, the three holelike bands significantly change. Note that the effect of including SO coupling on the band structure is qualitatively identical for all the functionals.

Compared to the LDA-SO band structure, the use of the mBJ exchange functional including SO interaction [right-hand panel on Fig. 1(a)] further leads to downward shifts of the holelike bands at Γ of up to 0.2–0.3 eV (label 1) and of lower lying bands (at ≈−2 eV) even more. For some *unoccupied* bands, the DFT-mBJ electronic structure results in an upwards shift of 0.1 eV (label 2). As a result there is a reduced band overlap of 0.4 eV of the hole and electron pockets at Γ and L, respectively [see Fig. 1(b)]. The GGA exchange-correlation functional (results not shown) already has the tendency in reducing the band overlap, compared to LDA, but of much smaller amplitude than mBJ. More generally, the effects related to the SO interaction and the negative and positive shifts of bands resulting from the use of mBJ are observable throughout the BZ [see Fig. 1(b) for band structure calculations along additional paths].

Let us now compare the DFT-calculated band structures with the spectra measured along the M-Γ (Fig. 2) and the

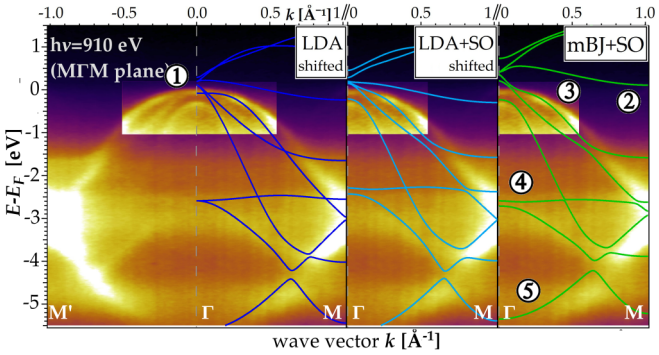

FIG. 2. (Color online) M'-Γ-M path. (Left) Measured data, region near E_F intensified. (Center and right) Measurement with calculations superimposed, from left to right LDA, LDA + SO, mBJ + SO, respectively, the former ones being shifted down by −0.3eV to make the comparison easier.

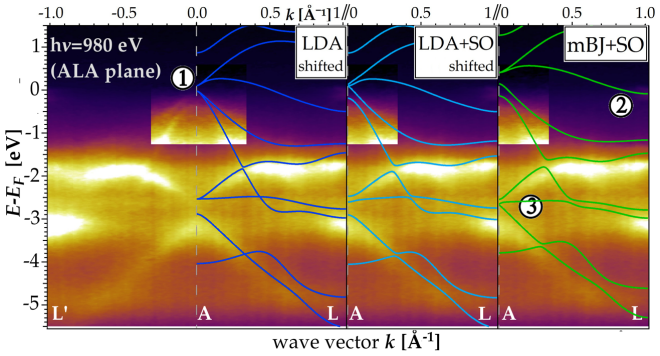

FIG. 3. (Color online) L'-A-L path. (Left) Measured data. (Center and right) Measurement with calculations superimposed, from left to right LDA, LDA + SO, and mBJ + SO, respectively, LDA and LDA + SO again shifted downwards by −0.3 eV.

L-A high symmetry lines (Fig. 3), as well as in the Γ-A-L-M plane, halfway between the Γ and A high-symmetry points of the BZ (Fig. 4). In Fig. 2, the experimental data obtained by probing the M′ΓM path of the BZ are compared with the different calculations. The band structure is symmetric for this path (see the BZ scheme, Fig. 1). The region, around Γ, close to E_F, is plotted with enhanced intensity and contains the top of the three (holelike) Se 4p bands. The panels show LDA, LDA + SO, mBJ + SO calculations (from left to right). Note that LDA and LDA + SO calculations are artificially shifted down by 0.3 eV to make their comparison easier. Despite the energy shift, it is clear that LDA is not reproducing the experiment very well at Γ close to E_F (see marker 1). The clear splitting of the lowest valence band observed in the experiment is not reproduced and only occurs in the LDA-SO calculation (see middle panel), clearly demonstrating the significant role of SO interaction in 1T-$TiSe_2$.

In the last panel of Fig. 2, the comparison is done using the mBJ functional with SO coupling. There is no more need for the artificial shifting of the band structure. The conduction band (not visible in the experiment) lies above E_F in mBJ + SO (marker 2) and the three Se 4p bands are better described than in the LDA + SO case since the topmost theoretical one at Γ reaches slightly further out in direction of M than for LDA + SO (marker 3). Also, the band at about

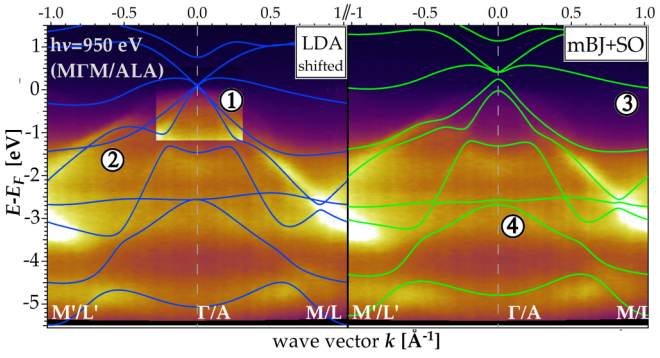

FIG. 4. (Color online) Measurement with a photon energy corresponding to a cut between Γ and A, compared with the LDA (blue) and mBJ + SO (green) calculations halfway between Γ and A. The LDA calculation is shifted downwards by −0.3 eV.

−2.5 eV (marker 4) is lower in energy, in good agreement with the measured data. On the other hand the lowest measured band (around −5 eV, marker 5) has a better curvature than LDA + SO but may be placed a bit too high in energy compared to the experiment. However, overall, the use of mBJ + SO leads to a good reproduction of the experimental band structure.

Note that for all exchange-correlation functionals, the maximum of the two topmost Se 4p bands is at higher energy than in the experiment. A likely explanation is given by the presence of strong electron-hole interactions in 1T-$TiSe_2$ [7,26,27], leading to a strong renormalization of the top of the valence band. This is further supported by the *ab initio* GW many-body theoretical study of the $TiSe_2$ band structure of Cazzaniga *et al.* [28], which has shown that the highest valence and lowest conduction bands are indeed strongly renormalized, in good agreement with the flattening of the topmost valence bands near Γ shown in the experiment. Such correlations are not considered in DFT-based calculations.

In fact, the major effect of GW compared to DFT-mBJ is that for GW, a small indirect gap effectively opens, leaving E_F at the top of the holelike bands at Γ (in agreement with experiment, Fig. 2) and the bottom of the electronlike band at L ∼ 0.2 eV above E_F. However, whereas the bottom of the bands for GW reaches down to almost −6 eV, DFT-mBJ, with −5.3 eV, is in better agreement with experiment. Furthermore, the flat band between −2 and −3 eV (Figs. 1 and 2, marker 4) does not change its energy between GW and DFT-LDA (see Ref. [28]). The calculation with DFT-mBJ, on the other hand, appears shifted down for a much better agreement with experiment (Fig. 2, marker 4). Therefore GW acts better close to E_F but overestimates the total band width whereas DFT-mBJ does not renormalize close to E_F but only slightly underestimates the total band width.

From the experimental point of view, the semimetal versus semiconductor question is discussed controversially (for details see Ref. [29]). Indeed, the presence of a band gap in the GW scheme indicates the presence of electron correlations. Therefore an approach going deeper than the conventional discussion in terms of δ-function bands is required since the electron spectral function (measured by ARPES) is renormalized by the correlation effects and even an intrinsic semiconductor band structure can end up with incoherent spectral weight crossing the Fermi level [29].

Figure 3 shows the SX-ARPES data corresponding to the L'-A-L path along which the band structure is also symmetric [see Fig. 1(a)]. The region near E_F is enhanced in intensity for better visibility and the panels show LDA, LDA + SO, mBJ + SO calculations (respectively from left to right). Again, both LDA and LDA + SO (first and second panel) need to be artificially shifted downwards (by −0.3 eV) for a comparison with the measured data. In this part of the BZ only the two topmost holelike Se 4p bands remain close to E_F because of the strong 3D character (k_z dispersion) of the third one [see Fig. 1 (b)] whose maximum is shifted down by approximately 2.5 eV.

The importance of SO interaction is also clearly evidenced in the experiment, since it shows a clear separation of the two remaining bands (marker 1), which is only reproduced by the calculations including SO. The comparison with bands at higher binding energies seems to ask for a slightly larger

downwards shift. However, a larger shift would hamper the comparison with the bands at Γ. This discrepancy is also present in the case of the mBJ + SO calculation (rightmost panel), although the bands are not artificially shifted in this case. Here again, it shows that the overall bandwidth is not perfectly reproduced by the DFT calculation and that the band structure is renormalized. The position of the valence band (marker 2) is higher in the mBJ + SO calculation than for LDA + SO and agrees better with experiment. On the other hand, the band crossing at about −2.5 eV at A (marker 3) does not fit to the measured data so well. Possibly, structural parameters of the calculations would have to be optimized, but this is beyond the scope of the present paper.

Figure 4 finally shows the comparison between experiment and theory for a cut through the BZ in the Γ-A-L-M plane halfway between Γ and A. Here the band structure is asymmetric]see BZ scheme in Fig. 1(a)]. Apart from this asymmetry, which is nicely reproduced by the calculation, the comparison leads to similar conclusions to those obtained for the M'-Γ-M and L'-A-L paths. LDA (blue) and LDA + SO (not shown) again need to be shifted artificially and the calculations performed without SO interaction lead to a poor agreement with the overall experimental band structure (markers 1 and 2). A splitting of the topmost two Se 4p bands is clearly necessary, as it happens in the calculation when SO coupling is introduced while moving from the left to the right panel in Fig. 4. The mBJ potential is still better than the shifted LDA especially in terms of the position of the conduction band (marker 3), which is higher for mBJ (just above E_F) and not seen in measured data. Also the band at about −3 eV (marker 4) is lower and thus corresponds better to the experiment for mBJ.

IV. CONCLUSION

The electronic structure of 1T-$TiSe_2$ has been investigated combining SX-ARPES experiments and DFT calculations using different exchange-correlation functionals. The experiments show a strong dependence on the photon energy demonstrating that this quasi-2D material has bands with 3D character (k_z dependent band structure) and that SX-ARPES is an excellent method for probing the 3D band structure. From the calculations and their comparison with experiment it becomes evident that SO coupling plays an important role in 1T-$TiSe_2$ and that the choice of the exchange-correlation functional is crucial for a good description of the electronic structure.

The importance of SO coupling is most apparent close to Γ and E_F where it introduces a splitting of the holelike Se p bands. Concerning the exchange-correlation functional, the use of mBJ + SO gives good energy positions, whereas LDA + SO consistently had to be shifted to lower energies. Although the agreement is not perfect, the mBJ + SO succeeds in describing most of the electronic band structure of 1T-$TiSe_2$. Discrepancies are observed at the top of the valence band, where specific electron-hole correlations (not considered in DFT) are expected to play an important role. As expected from the use of the mBJ potential for semiconductors, the tendency to increase the separation of valence and conduction bands has been also observed for 1T-$TiSe_2$.

ACKNOWLEDGMENTS

Skillfull technical assistance was provided by the workshop and electric engineering team. This work was supported by the Fonds National Suisse pour la Recherche Scientifique through Div. II. E.F.S acknowledges financial support from the JSPS postdoctoral fellowship for overseas researchers as well as the Alexander von Humboldt Foundation (Grant No. P13783). C.M. acknowledges support by the Swiss National Science Foundation under grant number PZ00P2_154867. The experiments were performed at the ADRESS beam line of the Paul Scherrer Institut, Switzerland.

[1] A. Soumyanarayanan, M. M. Yee, Y. He, J. van Wezel, D. J. Rahn, K. Rossnagel, E. W. Hudson, M. R. Norman, and J. E. Hoffman, Pro. Natl. Acad. Sci. USA **110**, 1623 (2013).

[2] F.-C. Hsu, J.-Y. Luo, K.-W. Yeh, T.-K. Chen, T.-W. Huang, P. M. Wu, Y.-C. Lee, Y.-L. Huang, Y.-Y. Chu, D.-C. Yan, and M.-K. Wu, Pro. Natl. Acad. Sci. USA **105**, 14262 (2008).

[3] F. J. Di Salvo, D. E. Moncton, and J. V. Waszczak, Phys. Rev. B **14**, 4321 (1976).

[4] F. Clerc, C. Battaglia, M. Bovet, L. Despont, C. Monney, H. Cercellier, M. G. Garnier, P. Aebi, H. Berger, and L. Forró, Phys. Rev. B **74**, 155114 (2006).

[5] J. A. Wilson, Solid State Comm. **22**, 551 (1977).

[6] C. Monney, E. F. Schwier, M. G. Garnier, N. Mariotti, C. Didiot, H. Beck, P. Aebi, H. Cercellier, J. Marcus, C. Battaglia, H. Berger, and A. N. Titov, Phys. Rev. B **81**, 155104 (2010).

[7] H. Cercellier, C. Monney, F. Clerc, C. Battaglia, L. Despont, M. G. Garnier, H. Beck, P. Aebi, L. Patthey, H. Berger, and L. Forró, Phys. Rev. Lett. **99**, 146403 (2007).

[8] A. F. Kusmartseva, B. Sipos, H. Berger, L. Forró, and E. Tutis, Phys. Rev. Lett. **103**, 236401 (2009).

[9] E. Morosan, H. W. Zandbergen, B. S. Dennis, J. W. G. Bos, Y. Onose, T. Klimczuk, A. P. Ramirez, N. P. Ong, and R. J. Cava, Nat. Phys. **2**, 544 (2006).

[10] J. Ishioka, Y. H. Liu, K. Shimatake, T. Kurosawa, K. Ichimura, Y. Toda, M. Oda, and S. Tanda, Phys. Rev. Lett. **105**, 176401 (2010).

[11] J.-P. Castellan, S. Rosenkranz, R. Osborn, Q. Li, K. E. Gray, X. Luo, U. Welp, G. Karapetrov, J. P. C. Ruff, and J. van Wezel, Phys. Rev. Lett. **110**, 196404 (2013).

[12] J. van Wezel, Europhys. Lett. **96**, 67011 (2011).

[13] K. Rossnagel, J. Phys.: Condens. Matter **23**, 213001 (2011).

[14] T. Pillo, J. Hayoz, H. Berger, F. Lévy, L. Schlapbach, and P. Aebi, Phys. Rev. B **61**, 16213 (2000).

[15] V. N. Strocov, X. Wang, M. Shi, M. Kobayashi, J. Krempasky, C. Hess, T. Schmitt, and L. Patthey, J. Synchrotron Rad. **21**, 32 (2014).

[16] V. N. Strocov, J. Electron. Spectroscop. Relat. Phenom. **130**, 65 (2003).

[17] V. N. Strocov, M. Shi, M. Kobayashi, C. Monney, X. Wang, J. Krempasky, T. Schmitt, L. Patthey, H. Berger, and P. Blaha, Phys. Rev. Lett. **109**, 086401 (2012).

[18] M. Tinkham, *Group Theory and Quantum Mechanics* (Courier Dover, 2003).

[19] F. Clerc, M. Bovet, H. Berger, L. Despont, C. Koitzsch, O. Gallus, L. Patthey, M. Shi, J. Krempasky, M. G. Garnier, and P. Aebi, J. Phys.: Condens. Matter **16**, 3271 (2004).

[20] Z. Zhu, Y. Cheng, and U. Schwingenschlögl, Phys. Rev. B **85**, 245133 (2012).

[21] P. Blaha, K. Schwarz, G. K. H. Madsen, D. Kvasnicka, and J. Luitz, *WIEN2K, An Augmented Plane Wave + Local Orbitals Program for Calculating Crystal Properties* (Karlheinz Schwarz, Techn. Universität Wien, Austria, 2001).

[22] J. P. Perdew and Y. Wang, Phys. Rev. B **45**, 13244 (1992).

[23] F. Tran and P. Blaha, Phys. Rev. Lett. **102**, 226401 (2009).

[24] Z. Zhu, Y. Cheng, and U. Schwingenschlögl, Phys. Rev. Lett. **110**, 077202 (2013).

[25] P. Villars and L. D. Calvert, *Pearson's Handbook of Crystallographic Data for Intermetallic Phases* (American Society for Metals Metals Park, OH, 1985), Vol. 2.

[26] C. Monney, E. F. Schwier, M. G. Garnier, N. Mariotti, C. Didiot, H. Cercellier, J. Marcus, H. Berger, A. N. Titov, H. Beck, and P. Aebi, New J. Phys. **12**, 125019 (2010).

[27] C. Monney, H. Cercellier, F. Clerc, C. Battaglia, E. F. Schwier, C. Didiot, M. G. Garnier, H. Beck, P. Aebi, H. Berger, L. Forró, and L. Patthey, Phys. Rev. B **79**, 045116 (2009).

[28] M. Cazzaniga, H. Cercellier, M. Holzmann, C. Monney, P. Aebi, G. Onida, and V. Olevano, Phys. Rev. B **85**, 195111 (2012).

[29] G. Monney, C. Monney, B. Hildebrand, P. Aebi, and H. Beck, Phys. Rev. Lett. **114**, 086402 (2015).